PREDICTIVE STUDY OF NON-AXISYMMETRIC NBI LOSS ON THE UPGRADED KSTAR PLASMA-FACING COMPONENTS

[1†]T. MOON, [2]T. RHEE, [2]J.-M. KWON, [2]Y.-M. JEON, [1§]E.S. YOON
[1]Ulsan National Institute of Science and Technology, Ulsan, Republic of Korea
[2]Korea Institute of Fusion Energy, Daejeon, Republic of Korea
†Speaker: tmoon@unist.ac.kr
§ Corresponding author: esyoon@unist.ac.kr

TH-H
30th IAEA FEC, Chengdu, 13th June ~ 18st Oct. 2025 ID:2916

ABSTRACT

CAD geometry supports engineering-level fidelity in NBI-induced ion-loss analysis

Using a KSTAR PFC CAD geometry and an efficient 3D collision-detection routine, we found (Fig. 1):

- **Diagonal, band-like, and non-axisymmetric** ion loss distribution by the combined poloidal turn and toroidal drift of fast ions.
- **Localized heat flux peaks** at protrusions and **leading edges** of the tungsten divertor.

Parameter scan over NB source (beam path), energy, and magnetic equilibrium

- Observed results can suggest ion loss mitigation guidance (limited to scanned range).

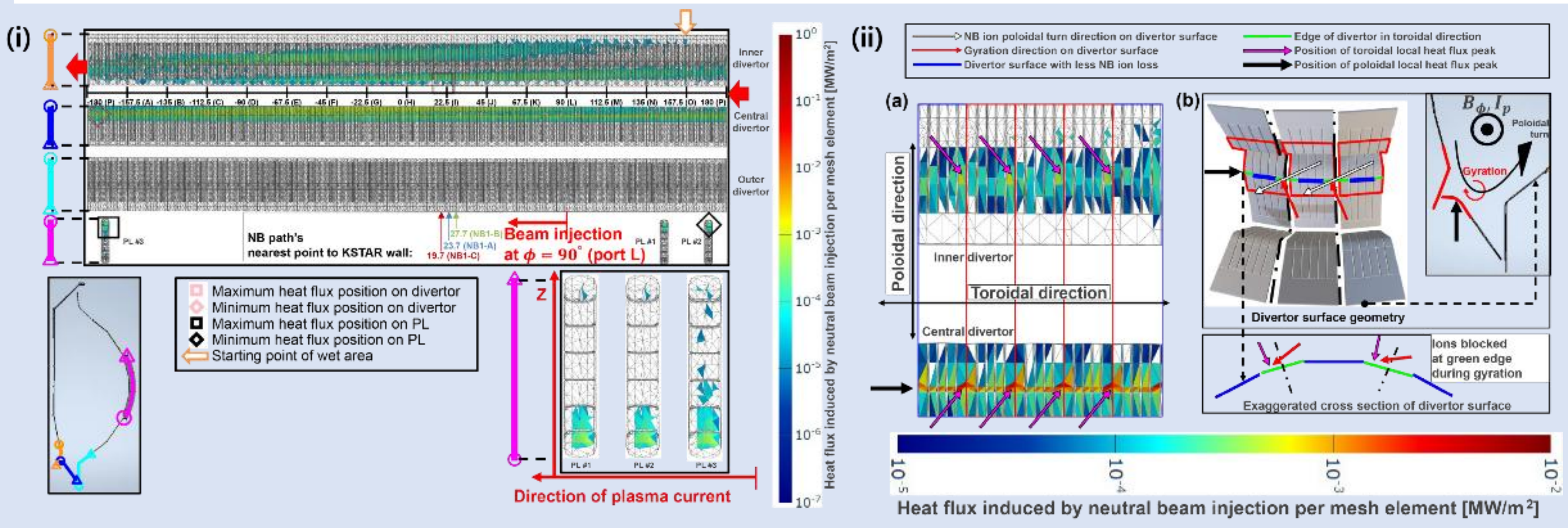

FIG. 1. (i) NuBDeC heat-flux map on unfolded divertor and PL surfaces for the reference case (100 keV NB1-C; equilibrium I in Fig. 2-i). (ii-a) Zoom of the inner/central divertor at 130–160° toroidal angle. (ii-b) 3D view of inner, central, and outer divertors; red outlines correspond to the three red rectangles in (ii-a).

BACKGROUND

- NBI heating generates fast ions; a fraction escapes confinement and deposits heat flux on PFCs, risking localized overheating [1-3].
- Accurate heat-load modeling requires geometry fidelity: early axisymmetric (2D poloidal) vessels were common [4, 5], whereas recent work adopts full 3D CAD models for higher-fidelity predictions [1, 6].
- CAD-to-simulation pipelines bring engineering-level geometry into synthetic diagnostics and integrated modeling frameworks for various fusion devices (W7-X, MAST-U, AUG, KSTAR, VNS and so on.) [7-11].
- High-fidelity geometry aids systematic detection of subtle but critical defects and ties model predictions to actionable engineering safeguards [12, 13].

METHODS

Monte Carlo orbit-following NuBDeC code for NBI simulation.

- Bi-Gaussian NB source is used. Ionization is sampled via the random-threshold method [14, 15].

Orbit integration: full Lorentz motion with gyration (RK4): $\dot{\mathbf{x}} = \mathbf{v},\ \dot{\mathbf{v}} = (\mathbf{q}/\mathbf{m})\mathbf{v} \times \mathbf{B},\ \mathbf{E} = 0$

- $\mathbf{B}$ is the magnetic equilibrium field (from equilibrium file); q/m is the charge-to-mass ratio.

CAD-to-simulation KSTAR PFC mesh + fast-ion path

- At each time step, the straight path segment between successive ion positions is tested against a CAD-derived PFC triangle mesh to record wall hits (Fig. 2-iii). Defeatured KSTAR PFC surfaces were tessellated into an unstructured mesh (376,747 triangles; 5-cm mesh size).

Two-phase 3D collision detection

- Space partitioning eliminates almost all non-colliding triangles with simple arithmetic (≈99.9% culled) → An exact segment–triangle test confirms hits on the few candidates; full workflow and algorithms are summarized in [16, 17].

Heat flux due to NBI-induced fast ion loss (Γ_j)

- On intersection with triangle j, the i-th sample ion's kinetic energy E_i is deposited on that element and recorded to its PFC region (divertor, PL, other; shown in Fig. 2-iii).
- For a beam pulse of duration Δt, the NBI-induced ion-loss heat flux on element j is:

$$E_i = \frac{1}{2}\omega_i m_i\left(v_{i,\parallel}^2 + \frac{2\mu_i B}{m_i}\right),\ \Gamma_j = \sum_i \frac{E_i}{A_j \Delta t},\ (A_j\text{: triangle area, } \omega_i\text{: particle weight.})$$

SIMULATION SETUPS & RESULTS

- **Scan space**: KSTAR NB1-A/B/C sources; beam energy = 60 or 100 keV; equilibrium: $\{I_p$: 0.50/0.75/1.00 MA; β_p: 1.0/2.0; two strike point configurations$\}$ (Fig. 3-i).
- For **beam deposition** calculations, **electron density** and **temperature profiles** are in Fig. 3-ii (typical KSTAR H-mode profiles).
- Magnetic **ripple** effects are **neglected** (approximately 0.04% amplitude).
- Each setup tracks 2.4 × 10^6 Monte Carlo sample ion particles.
- **Summary of the results: Ion-loss heat flux and power fraction ranges (42 setups; 1 MW NBI; Fig. 3)**
  - Divertor: heat flux max. < ≈30 kW m^{-2}; power fraction < 0.5%
  - PL: heat flux max. < ≈40 kW m^{-2}; power fraction < 0.3%
  - Other PFCs: heat flux max. < ≈15 kW m^{-2}; power fraction < 0.35%

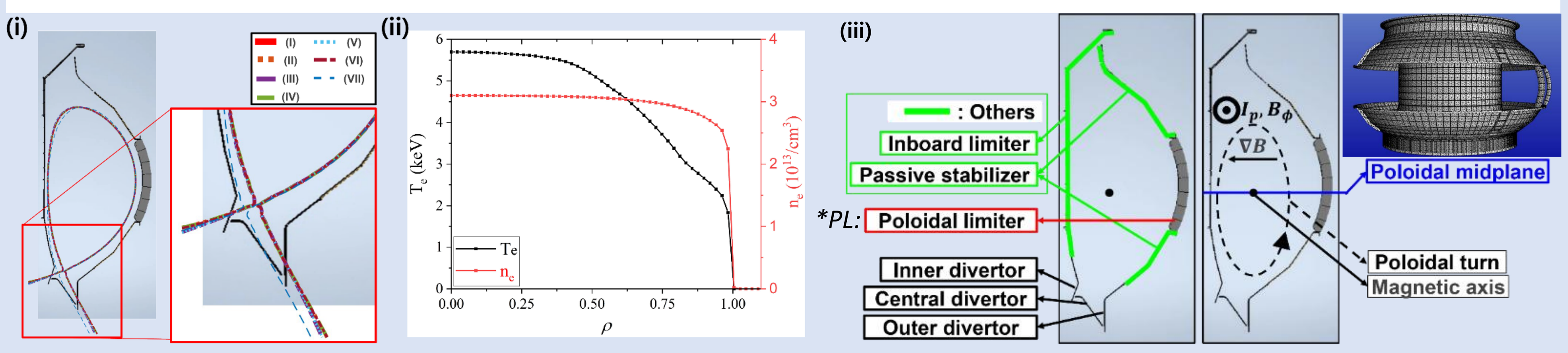

FIG. 2. (i) Toroidal cross section of magnetic separatrices for seven magnetic equilibria in the NuBDeC simulation parameter scan. Equilibrium case I is the reference setup ($I_p = 1.00\ MA, \beta_p = 1.0$). (ii) One-dimensional profiles of electron temperature (T_e) and density (N_e) over $\rho = \sqrt{\psi_N} = \sqrt{(\psi - \psi_{\text{axis}})/(\psi_{LCFS} - \psi_{\text{axis}})}$.
*(iii) Toroidal cross section of KSTAR PFC surfaces illustrating the poloidal turn, poloidal midplane, and the following PFC regions. Categorization of the simulation results: divertor, *PL, and others.*

ACKNOWLEDGEMENTS AND REFERENCES

- This work was supported by the National Research Foundation of Korea (NRF) grant funded by the Korea government (MSIT) (No. RS-2023-00254695). Computing resources were provided on the KFE computer, KAIROS, funded by the Ministry of Science and ICT of the Republic of Korea (KFE-EN2541-11).

[1] WARD, S. H., *et al.*, *Nucl. Fusion* **62** 12 (2022) 126014.
[2] KURKI-SUONIO, T., *et al.*, *J. Plasma Phys.* **84** 6 (2018) 745840603.
[3] AKERS, R., *et al.*, 26th IAEA FEC (Proc. Int. Conf. Kyoto, Japan, 2016), IAEA, Vienna (2016).
[4] KIM, J. Y., *et al.*, *AIP Adv.* **6** 10 (2016) 105013.
[5] BAK, J., *et al.*, *Nucl. Mater. Energy* **12** (2017) 1270–1276.
[6] ÄKÄSLOMPOLO, S., *et al.*, *Nucl. Fusion* **58** 8 (2018) 082010.
[7] LEVINESS, A., *et al.*, *Nucl. Fusion* **64** 9 (2024) 096034.
[8] VELARDE, L., *et al.*, *Plasma Phys. Control. Fusion* **67** 1 (2024) 015024.
[9] LUNT, T., *et al.*, *Phys. Rev. Lett.* **130** 14 (2023) 145102.
[10] KWON, J.-M., *et al.*, IEEE *Trans. Plasma Sci.* **52** 9 (2024) 3910–3916.
[11] FRANKE, T., *et al.*, *Fusion Eng. Des.* **215** (2025) 115035.
[12] JUAREZ, R., *et al.*, *Nat. Energy* **6** 2 (2021) 150–157.
[13] JUAREZ, R., *et al.*, *Nat. Commun.* **15** 1 (2024) 8563.
[14] NA, B., *et al.*, *Fusion Eng. Des.* **185** (2022) 113320.
[15] RHEE, T., *et al.*, *Phys. Plasmas* **26** 11 (2019) 112504.
[16] MOON, T., *et al.*, *Comput. Phys. Commun.* **309** (2025) 109490.
[17] ERICSON, C., *CRC Press*, "Boca Raton" (2004).

PARAMETER-DRIVEN CHANGES IN ION-LOSS DISTRIBUTION

Beam energy and source (Figs. 3-5)

- 100 → 60 keV: poloidal wetting narrows; peak heat flux ↓ ≈75–80%; deposited power fraction ↓ ≈90–95%.
- NB1-C: highest losses; NB1-A: 3–4 times lower than NB1-C; NB1-B: no measurable losses.

Plasma current and poloidal beta

- I_p↓ → higher safety factor (q) and stronger radial drift → broader distribution along poloidal-turn (Fig. 6-ii-d).
- β_p↑ (Shafranov shift) → increased divertor and PL deposition (Fig. 3).

Strike-point relocation

- Moving the outer strike point to the central divertor → divertor wetted area is expanded; Deposition expands to inboard limiter; PL wetting shifts to higher Z.
- Produces broader ion-loss distribution changes than β_p variations (Fig. 5-i-e, 5-ii).

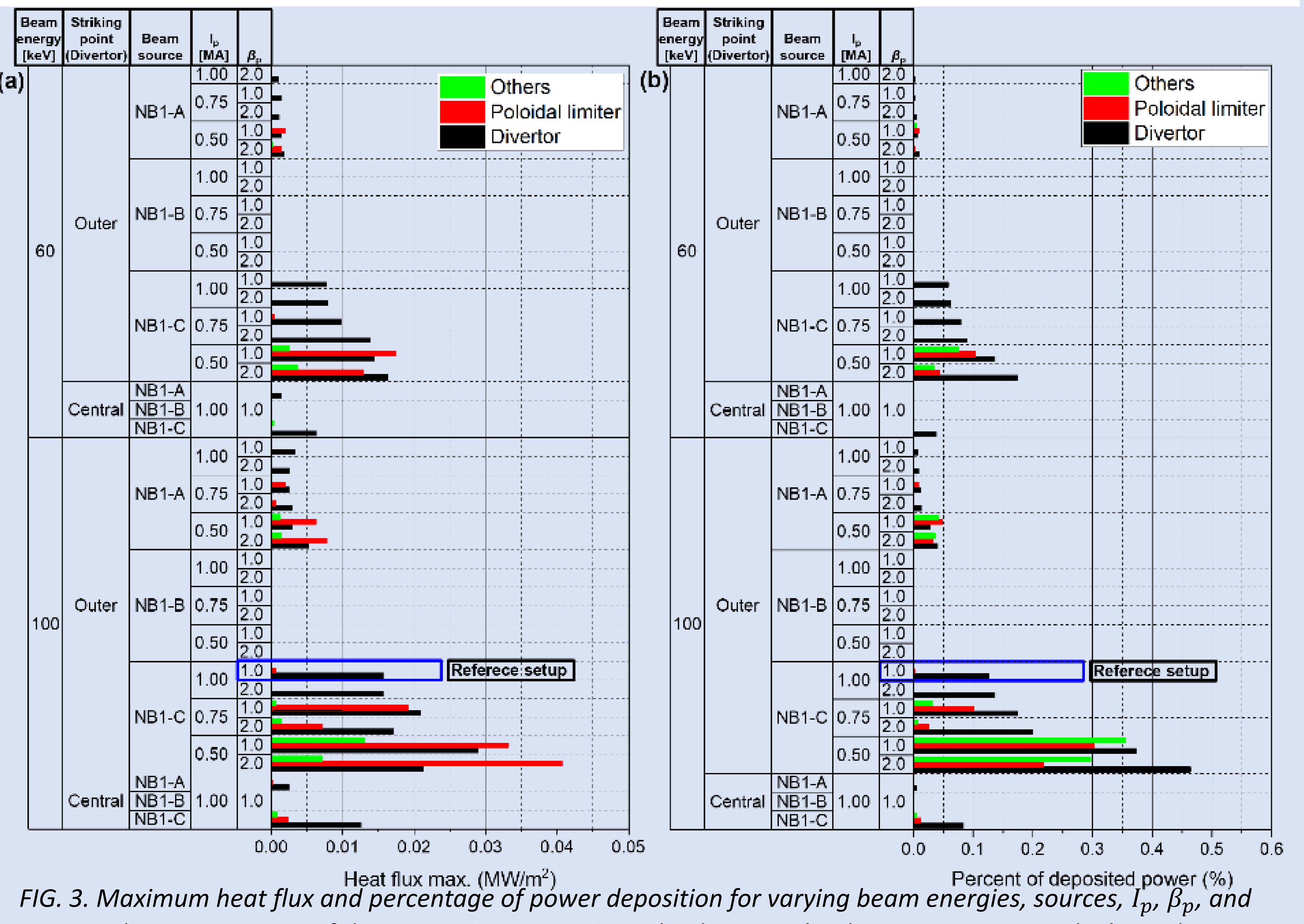

FIG. 3. Maximum heat flux and percentage of power deposition for varying beam energies, sources, I_p, β_p, and outer strike point position of the magnetic separatrix on the divertor. The three PFC regions in the legend are illustrated in Fig. 2-iii.

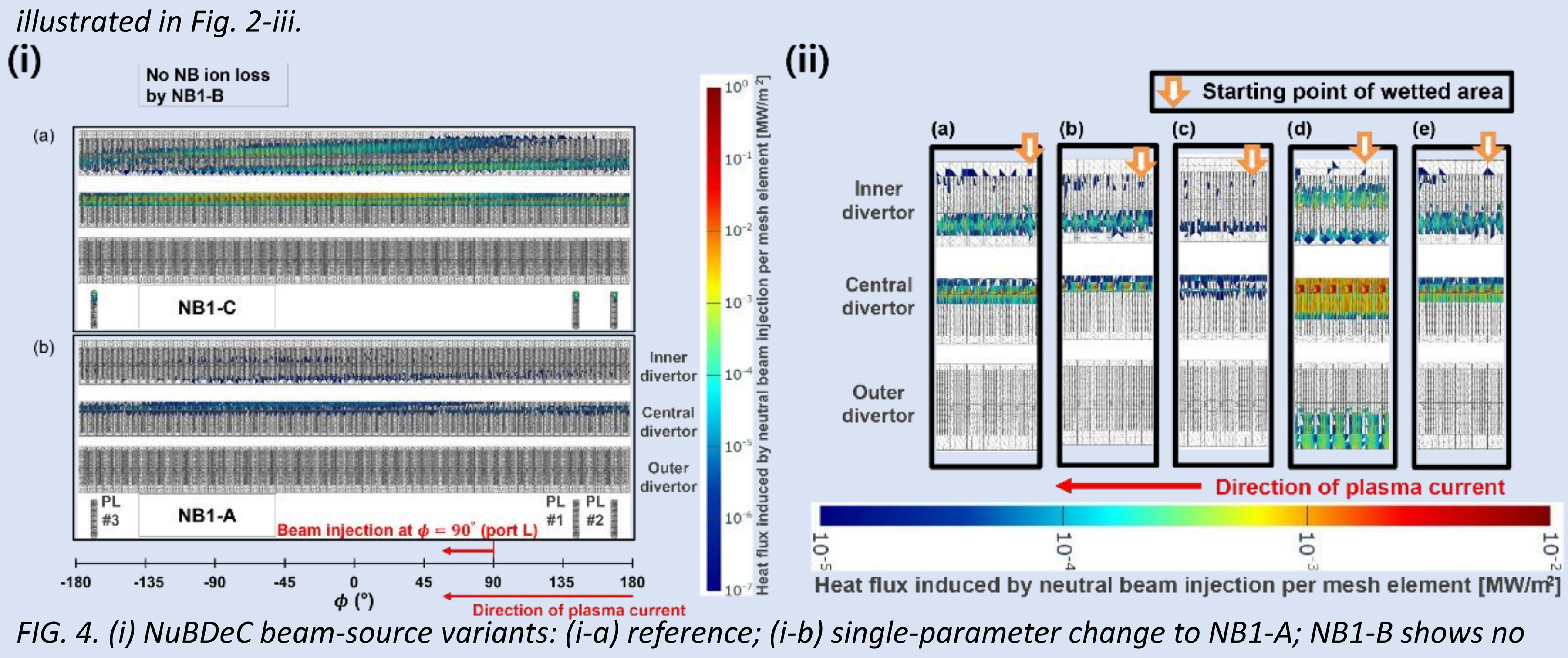

FIG. 4. (i) NuBDeC beam-source variants: (i-a) reference; (i-b) single-parameter change to NB1-A; NB1-B shows no ion loss. (ii) Heat-flux maps from ion loss on the unfolded divertor: (ii-a) reference; (ii-b) 60 keV; (ii-c) NB1-A; (ii-d) I_p = 0.50 MA; (ii-e) β_p = 2.0. The white arrow (orange outline) marks the start of the plasma-wetted area.

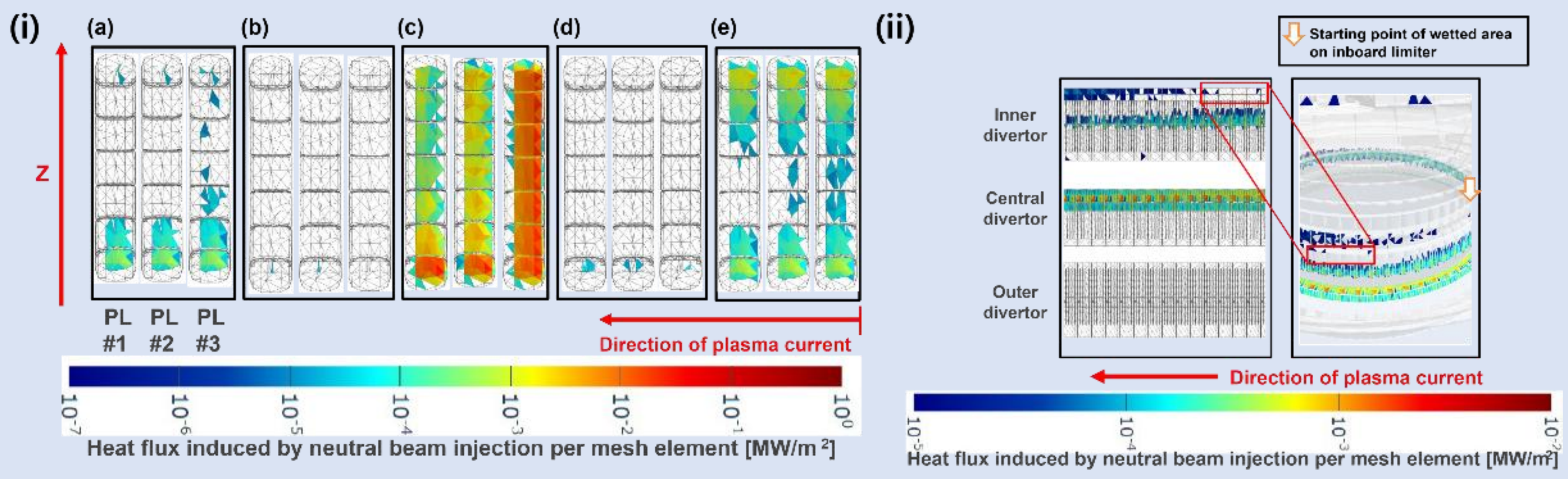

FIG. 5. (i) Unfolded-PL heat-flux maps from NuBDeC NBI-induced ion loss: (i-a) reference; single-parameter variants—(i-b) NB1-A source, (i-c) I_p = 0.50 MA, (i-d) β_p = 2.0, (i-e) outer separatrix strike on the central divertor. PL heat flux vanishes for 60 keV NB1-C. (ii) Unfolded-divertor map for the outer strike on the central divertor (cf. Fig. 4-ii); the wetted area reaches the inner limiter. The white arrow (orange outline) marks the start of the plasma-wetted area.

DISCUSSION AND CONCLUSION

- CAD-based NBI simulation predicts non-axisymmetric, geometry-sensitive heat-flux bands with peaks at toroidal leading edges and upstream KSTAR PFC surfaces.
- Across 42 setups: divertor/PL ion-loss heat flux max. remain < 30–40 kW m^{-2} with sub-percent power fractions.
- Three of the main factors that control the heat flux patterns are analyzed:
  1. (Beam deposition location) Deposition (ionization) sets the poloidal-turn and loss position. NB injection close to high-field side (HFS)→ deposition close to HFS; changes in I_p, β_p reshape flux surfaces → deposition shifts.
  2. (Magnetic geometry shifts) Moving flux surfaces or the outer strike point repositions losses even for the same deposition, by changing ion loss distribution.
  3. (Radial drift scaling) Drift grows with higher beam energy ($v_\parallel$↑) and lower I_p (q↑), broadening the ion loss distribution and raising divertor loading.
- This workflow can provide a systematic basis to tune NBI and mitigate localized hot spots. The resulting heat-flux datasets are visualization-ready in virtual environments such as the V-KSTAR platform and are intended for further use in synthetic diagnostics and integrated simulation, providing engineering-level fidelity and seamless geometrical context on which the data can be mapped.
- For the future work, non-axisymmetric fields (e.g., RMP), MHD instabilities, and atomic processes (thermalization, charge-exchange) will be considered.